Chapter 9

MRI Mapping of Renal T_1: Basic Concept

Stefanie J. Hectors, Philippe Garteiser, Sabrina Doblas, Gwenaël Pagé, Bernard E. Van Beers, John C. Waterton, and Octavia Bane

Abstract

In renal MRI, measurement of the T_1 relaxation time of water molecules may provide a valuable biomarker for a variety of pathological conditions. Due to its sensitivity to the tissue microenvironment, T_1 has gained substantial interest for noninvasive imaging of renal pathology, including inflammation and fibrosis. In this chapter, we will discuss the basic concept of T_1 mapping and different T_1 measurement techniques and we will provide an overview of emerging preclinical applications of T_1 for imaging of kidney disease.

This chapter is based upon work from the COST Action PARENCHIMA, a community-driven network funded by the European Cooperation in Science and Technology (COST) program of the European Union, which aims to improve the reproducibility and standardization of renal MRI biomarkers. This introduction chapter is complemented by two separate chapters describing the experimental procedure and data analysis.

Key words Magnetic resonance imaging (MRI), Parametric imaging, T_1 mapping, Kidney, Preclinical

1 Introduction

Renal pathologies may result in structural and functional changes that could possibly be noninvasively detected by magnetic resonance imaging (MRI) [1]. While the MRI relaxometry parameter T_1, that is, the longitudinal relaxation time, is used quite extensively for assessment of other organs, for example in cardiac and brain MRI, its application for the assessment of renal pathology is relatively scarcely used. Several reports, both in the clinical [1] and preclinical setting [2–5], have shown promise of T_1 for detection and characterization of renal pathologies, including inflammation and fibrosis. These results warrant further investigation of this relaxation parameter for evaluation of renal pathology. In this chapter, we will discuss the basic concept of T_1 as well as emerging applications of this MRI parameter for noninvasive characterization of renal pathologies.

This introduction chapter is complemented by two separate chapters describing the experimental procedure and data analysis, which are part of this book.

Andreas Pohlmann and Thoralf Niendorf (eds.), *Preclinical MRI of the Kidney: Methods and Protocols*, Methods in Molecular Biology, vol. 2216, https://doi.org/10.1007/978-1-0716-0978-1_9,

This chapter is part of the book Pohlmann A, Niendorf T (eds) (2020) Preclinical MRI of the Kidney—Methods and Protocols. Springer, New York.

2 Measurement Concept

2.1 Basic Concept of T_1 Mapping

Magnetic resonance imaging (MRI) is based on the interaction of nuclear spins with three types of magnetic fields: main field B_0, radiofrequency field B_1, and linear gradient fields. MRI signal relies on the physical properties of atoms with an odd number of protons or neutrons, which possess a nuclear angular momentum (spin), that gives rise to a magnetic dipole moment. Using classical physics, the atom can be described as a charged sphere spinning about its axis and giving rise to a current loop that creates the magnetic dipole moment. Since MRI is concerned with the spin property of protons and neutrons, and their interactions with a large magnetic field, these particles will be referred to as "spins". Most MRI applications in biological specimens generate signal by manipulating the spin of single proton hydrogen (^1H), although it is feasible to generate MR images in biological samples from the signal of other nuclei such as sodium [6], or hyperpolarized gases.

$$\boldsymbol{\omega}_0 = \boldsymbol{\gamma}\, \mathbf{B}_0 \tag{1}$$

In the absence of a magnetic $\mathbf{B_0}$ field, nuclear spins are oriented randomly. The presence of an external magnetic field ($\mathbf{B_0}$) will have two effects on the spins: they will tend to align with the main magnetic field $\mathbf{B_0}$, to create a net macroscopic magnetic moment $\mathbf{M_0}$ in the direction of the field (the longitudinal direction, or conventionally, the z-direction), and they will precess around the main magnetic field at a well-defined frequency called the Larmor frequency (Eq. 1, Fig. 1) where γ, the gyromagnetic ratio, is a constant specific to each atom. Thus, a ^1H atom in a magnetic field of 1 tesla (T) = 10^4 gauss will precess about the field with a Larmor frequency of $\gamma/2\pi = 42.58$ MHz/tesla [7, 8].

The presence of the static magnetic field B_0 polarizes the sample of protons to a net magnetization $\mathbf{M_0}$ in the longitudinal direction. However, polarization is not sufficient to obtain a large, coherent MR signal for image reconstruction. To obtain the MR signal, a radiofrequency field $\mathbf{B_1}$ is applied as a pulse of a few milliseconds in the xy (transverse) plane. $\mathbf{B_1}$ is tuned to the resonant Larmor frequency of the spins, so it excites the spins out of equilibrium, tipping the $\mathbf{M_0}$ vector away from the z-axis by an angle known as flip angle, which is dependent on the amplitude and duration of the RF pulse (Fig. 2) [8]. The $\mathbf{B_1}$ induced rotation of the magnetization toward the transverse plane causes the longitudinal component of magnetization to decrease, and the transverse component to increase.

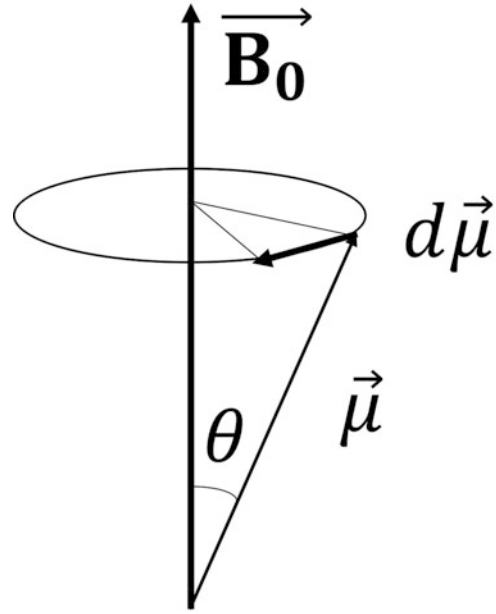

Fig. 1 B_0 interacts with the nuclear magnetic moment μ, producing a torque that causes the protons to precess around B_0. (From Dwight Nishimura, "Principles of Magnetic Resonance Imaging," Stanford University Press, Palo Alto, CA, 2010)

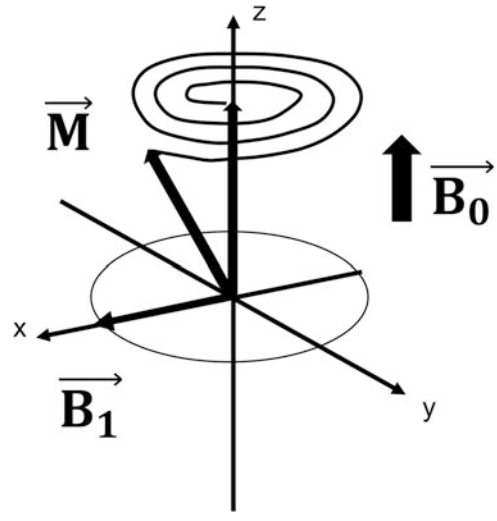

Fig. 2 Nutation at Larmor frequency of the magnetization vector around the RF pulse B_1 applied in the transverse plane. (From Dwight Nishimura, "Principles of Magnetic Resonance Imaging," Stanford University, Palo Alto, CA 2010)

When the RF $\mathbf{B_1}$ pulse is turned off, the magnetization precesses back to its equilibrium state, and the longitudinal component recovers, while the transverse component decays. The Bloch equation describes the behavior of the magnetization vector **M,** based on the T_1 and T_2 relaxation time constants and the magnetic fields applied:

$$\frac{d\mathbf{M}}{dt} = \mathbf{M} \times \gamma\mathbf{B} - \frac{M_x\mathbf{i} + M_y\mathbf{j}}{T_2} - \frac{(M_z - M_0)\mathbf{k}}{T_1} \quad (2)$$

Solving the z-axis component of the Bloch equation, we obtain an exponential expression for the recovery of M_z to the equilibrium M_0 magnetization (Eq. 3). The time constant T_1 is known as the spin-lattice or longitudinal relaxation time.

$$M_z(t) = M_0 + \left(M_{z\,(t=0)} - M_0\right) \exp\left(-\frac{t}{T_1}\right) \quad (3)$$

The reference standard method for measuring T_1 is the inversion-recovery spin echo method (IR-SE; see IR-SE signal curve in Fig. 3 top) that originated from early NMR experiments [9, 10]. It involves inversion of the magnetization M_0 by a 180° RF pulse in the z direction, followed by a time delay known as inversion time (TI) during which the equilibrium magnetization is allowed to decay. The TI ends after the application of a 90° RF pulse, which tips the magnetization in the x-y (transverse) plane for MR signal readout (receiving). A 180 pulse is then applied in the x direction, to rephase the precessing spins in a "spin echo" occurring at a fixed echo time TE.

After a long repetition time (TR) that allows for the magnetization to recover to equilibrium, the IR preparation is repeated with different subsequent inversion times. For accurate work, between 4 and 10 TI values should be used, although a T_1 can be calculated with as few as two TI values. TR is chosen to be much longer than the longest expected T_1 of interest in the tissue, in order to allow the magnetization to fully recover to equilibrium. For very accurate work this ratio TI/T_1 is as high as 5 or even 7, although for in vivo work 3 is more common. Signal decay and recovery can be observed on the images acquired with different TI's (Fig. 3 top), with signal nulling at $TI_{null} = T_1 \ln 2$, when the inversion preparation pulse is exactly 180° and the $TR >> T_1$ of tissue. If expected T_1 of the tissue is known, choosing a range of TI's before and after TI_{null} allows for acquisition of enough data points to fit the signal decay and recovery curve. Alternatively, performing a series of preliminary IR-SE experiments allows identification of the signal nulling time in the tissue of interest (TI_{null}), and choice of optimal range of TI values for measuring T_1.

IR-SE pulse sequences used currently in animal [2, 3] and human imaging differ from the reference standard IR-SE experiment described above by use of fast readout techniques. There are

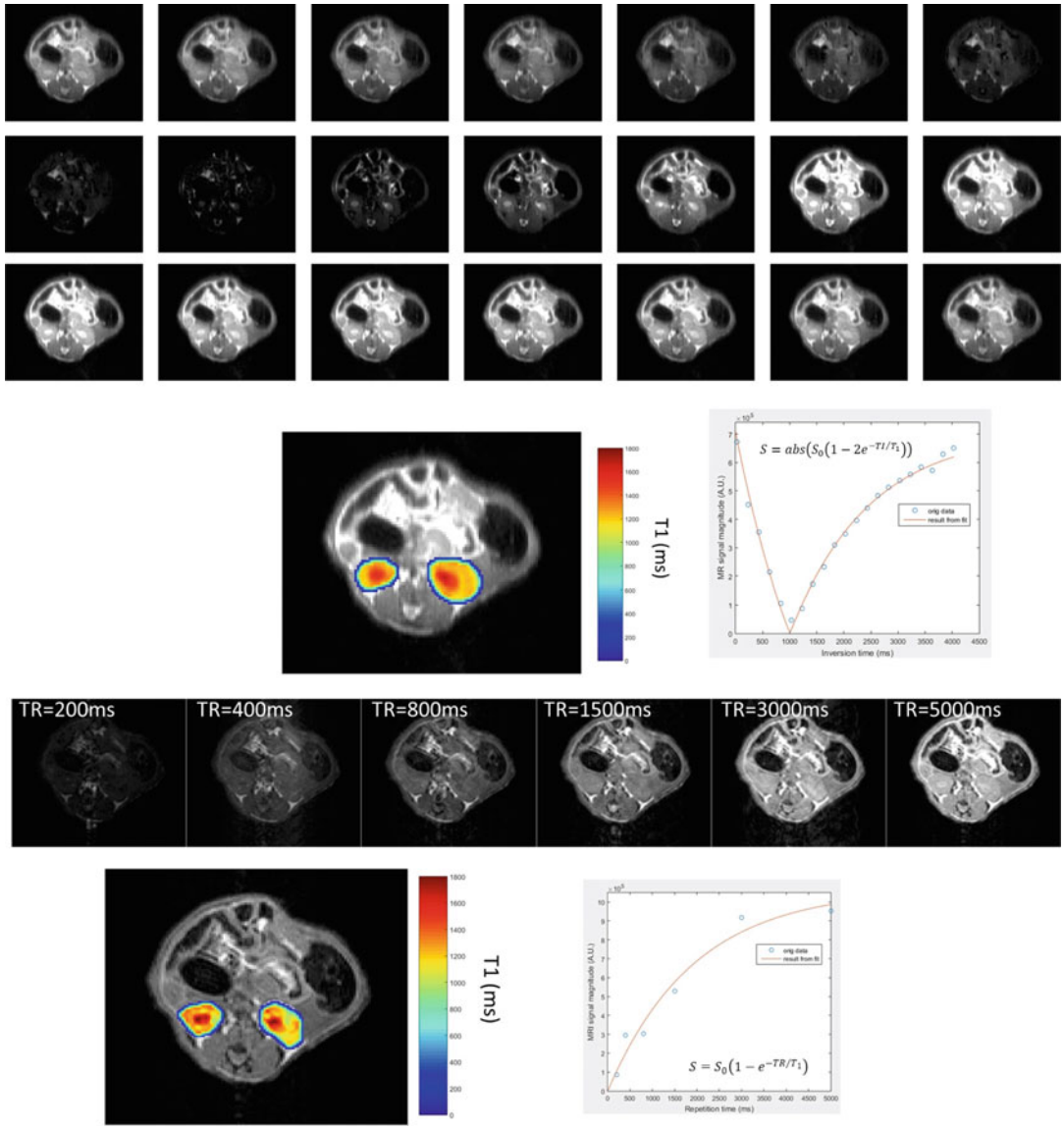

Fig. 3 T_1 mapping examples in the kidneys of a control mouse (c57bl6) imaged on a 7 T Bruker Pharmascan. Top: Inversion recovery experiment with a FAIR RARE pulse sequence, showing sequence of inversion times, T_1 color map and signal recovery curve: TE = 35.8 ms; recovery time = 10 s; NEX = 2; scan time 8 min 33 s; 21 inversion times (TI = 30 + $n \times$ 200 ms, $n = 0 \ldots 20$); nonselective inversion slice; matrix 128 $\times$ 100; FOV 40 $\times$ 30 mm; single 1 mm-thick slice. Bottom: Variable TR experiment with a RARE VTR pulse sequence, showing 8 variable repetition times (200, 400, 800, 1500, 3000, 5000 ms), T_1 color map and signal recovery curve: TE 11 ms; NEX = 1; scan time 8 min 43 s; matrix 128 $\times$ 96; FOV = 40 $\times$ 30 mm; single 1 mm-thick slice; no fat suppression; shallow breathing; no motion compensation

various fast readout techniques that have been introduced for both inversion and saturation recovery pulse sequences:

1. The **Ra**pid Imaging with **R**efocused **E**choes (RARE) readout, also called fast or turbo spin-echo readout by clinical scanner manufacturers, uses several 180° refocusing pulses within the same TR to create an echo train. Within the echo train, each 180 pulse induces a refocused echo, comprising spin-echo and stimulated echo contributions, which is digitized, and each echo is acquired with a different phase encoding gradient, so that multiple lines of k-space (multiple phase encoding steps) can be acquired within the same TR. The number of 180° pulses is called the echo train length (ETL) or RARE factor: a typical value is 8.
2. **E**cho **p**lanar **i**maging (EPI) uses a single RF preparation (in the case of IR, 180°-TI-90°) and then acquire multiple gradient echoes by combining a high amplitude bipolar oscillating frequency encoding gradient with a low amplitude monopolar blip phase encoding gradient. This approach permits fast acquisition of k-space data in a single shot (all lines of k-space in the 2D plane are acquired for each RF preparation), or a few multiple shots (groups of k-space lines are acquired for each RF preparation).
3. A derivative of the IR methods, the Look–Locker inversion recovery (LL-IR) method, samples the magnetization recovery using rapid, small flip angle imaging readouts. More details and caveats on data acquisition and analysis with this method can be found in the chapters by Garteiser P et al. "Experimental Protocols for MRI Mapping of Renal T_1" and "Analysis Protocols for MRI Mapping of Renal T_1." In addition to EPI, LL-IR pulse sequences can employ other readout methods:
   - **F**ast **l**ow **a**ngle **s**hots (FLASH) tips the magnetization to the transverse xy plane during the recovery period by a small angle, in order to sample it. Magnetization is spoiled before subsequent RF pulses. This readout method has the advantage of a short TR (~3 ms) that is compatible with low flip angles (<10°) [11]. As such, the longitudinal regrowth of the magnetization is perturbed only to a small extent. Use of a FLASH readout requires fitting the data with a modified version of the IR-SE equation, the Look–Locker equation (chapter by Garteiser P et al. "Analysis Protocols for MRI Mapping of Renal T_1"). FLASH can also be used in T_1 mapping methods that do not employ an inversion pulse, like variable flip angle (see next section).
   - Balanced readouts such as **s**teady-**s**tate **f**ree **p**recession (SSFP) can also be used, as they tend to yield higher signal to noise due to the reuse of magnetization from preceding shots [12]. Use of these types of readouts also requires

fitting the data with a Look–Locker equation or more complex equations that take into account the dependence of signal on both T_1 and T_2 decay. Details on acquisition and analysis with pulse sequences using an SSFP or FISP readout method can be found in the chapters by Garteiser P et al. "Experimental Protocols for MRI Mapping of Renal T_1" and "Analysis Protocols for MRI Mapping of Renal T_1."

2.2 Overview of T_1 Mapping Techniques

The longitudinal relaxation time T_1 can be measured by a variety of methods [13, 14]. The multiple delay inversion-recovery (IR) method can measure T_1 with high accuracy, however, it has long acquisition times (10–15 min with current EPI readouts [2, 3]), which makes it impractical for in vivo settings. There are several methods that have been developed for faster T_1 measurement: the saturation recovery or variable TR (VTR) method, the variable flip angle (VFA), the Look–Locker modified IR, and the proton density (PD) method. Comprehensive description of the most common pulse sequence implementations for each T_1 measurement method, acquisition protocols and corresponding analysis workflows for preclinical and clithe chapters by Garteiser P et al. "Experimental Protocols for MRI Mapping of Renal T_1" and "Analysis Protocols for MRI Mapping of Renal T_1."

2.2.1 The Saturation Recovery or VTR Method

The saturation recovery or variable TR (VTR) method, in which T_1-weighted signal is acquired with multiple TR values (Fig. 3b) shares the same limitations of limited spatial coverage and resolution as the IR method but allows shorter overall scan times [15]. The magnetization is tipped 90° (from the z to the xy plane) and the recovery is usually sampled by a RARE readout over several repetition times TR of different durations (Fig. 3b).

2.2.2 The VFA Method

In variable flip angle (VFA) methods [14–17], the RF flip angle is varied while keeping the TR constant in a 2D or 3D spoiled gradient echo (SPGR) acquisition. VFA is particularly useful in dynamic contrast-enhanced MRI (DCE-MRI) experiments, as VFA measurements allow for voxel-based baseline (precontrast enhancement) T_1 mapping with the same spatial resolution and coverage as the DCE-MRI scan in a short amount of time.

2.2.3 The Look–Locker Modified IR Method

The Look–Locker modified IR [18–21], decreases the acquisition time by sampling the signal recovery curve multiple times per TR after application of several low flip angle pulses during the acquisition. Despite shortened acquisition time, Look–Locker IR methods are still limited in spatial coverage.

2.2.4 The PD Method

In the proton density (PD) approach [22], T_1 is derived by comparing PD-weighted images with DCE baseline (precontrast) images acquired with an SPGR pulse sequence. More information on the use of T_1 for quantitative DCE-MRI measurements can be

found in the chapters by Li L-P et al. "MRI Mapping of the Blood Oxygenation Sensitive Parameter T_2* in the Kidney: Basic Concept"; by Chuang K-H et al. "Renal Blood Flow Using Arterial Spin Labeling (ASL) MRI: Experimental Protocol and Principles"; and by Grist JT et al. "Analysis Protocol for Renal Sodium (23Na) MR Imaging," which cover the basic concept, experimental protocols, and analysis techniques of DCE-MRI, respectively.

2.2.5 MR Fingerprinting

Next to conventional T_1 mapping techniques, T_1 can also be extracted from magnetic resonance fingerprinting techniques, a novel MRI method that uses a pseudorandomized acquisition scheme to generate unique signal evolutions (or "fingerprints") for each tissue voxel dependent on the relaxation parameters [23].

3 Overview of Applications on Preclinical and Clinical MR Instruments

T_1 differs between different kidney components (cortex, medulla, urine, etc.); it decreases when paramagnetic contrast agents such as gadolinium chelates or oxygen (O_2) are present, and it may increase or decrease with pathology. In addition T_1 tends to increase with B_0, an important consideration since animal studies have been performed over more than an order of magnitude range in B_0.

The sensitivity of T_1 to the tissue microenvironment has been employed quite extensively to assess renal structure and function, both in clinical and preclinical studies. A comprehensive review of clinical T_1 (and T_2) applications in the kidney can be found here [24]. The use of T_1 for noninvasive assessment of renal pathology in preclinical models has already been explored in the 1980s, showing that various effects including ischemia, tubular obstruction and renal congestion may attribute to T_1 differences in rat models of acute and chronic renal failure [25, 26]. T_1 values can be affected by a wide variety of changes in the tissue environment, including inflammation and fibrosis. Inflammation can coexist with fibrosis in the kidney tissue [27], for example during rejection of transplanted kidneys. While clinical MRI studies are valuable for, for example, the grading of renal fibrosis in patients, preclinical studies with well-established animal models have the advantage of the possibility to assess dynamic changes in T_1 after the onset of pathology.

Hueper et al. performed longitudinal T_1 measurements on a 7 Tesla dedicated animal MR scanner in mice after transient unilateral clamping of the renal pedicle, causing moderate or severe acute kidney injury (AKI) dependent on the ischemia time [3]. T_1 values were significantly elevated after AKI, with a peak at 7 days after the ischemic event. In mice with severe AKI, the T_1 elevation persisted until at least a month after surgery. The initial peak in T_1 values is likely attributed to increased water content due to an acute

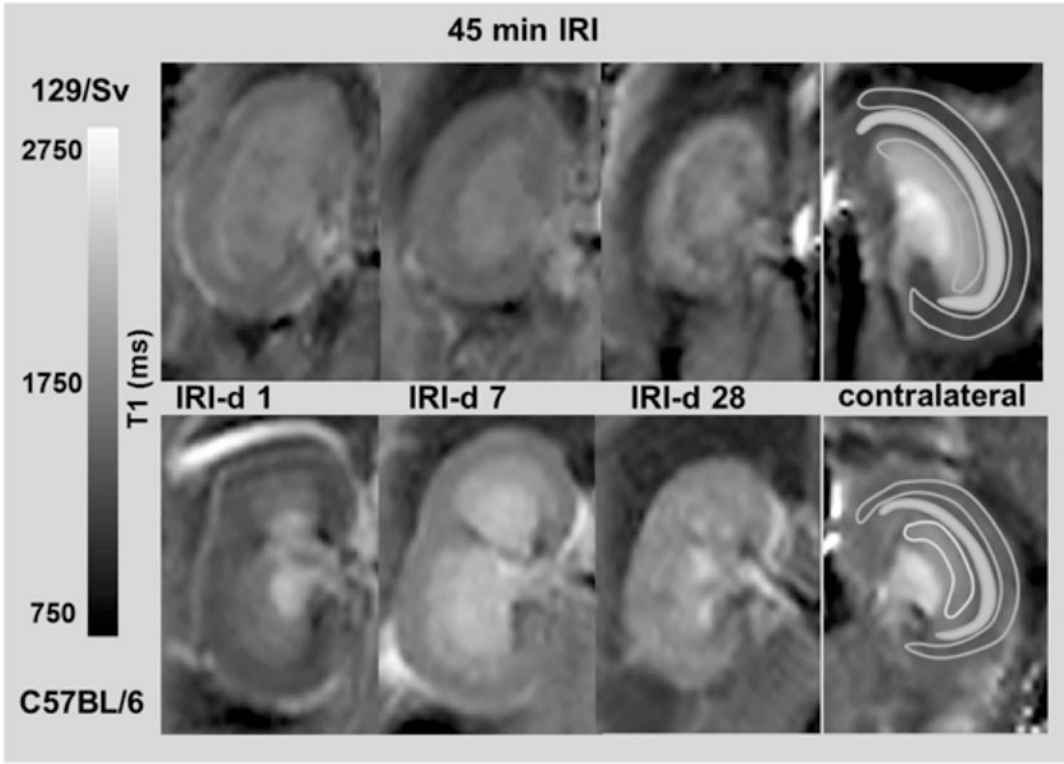

Fig. 4 T_1 maps after 45 min ischemia reperfusion injury (IRI) for 129/Sv (upper row) and C57BL/6 mice (lower row) at day 1, day 7 and day 28 are shown. In T_1 maps spatial differences can be measured by placing ROIs in the cortex and the outer stripe (OSOM) and inner stripe (ISOM) of the outer medulla, which is illustrated in the contralateral normal kidney. After severe acute kidney injury, differences of T_1-values between the two mouse strains were most pronounced on day 7: this example shows higher T_1-values in the ISOM and lower T_1-values in the renal cortex of C57BL/6 compared to 129/Sv mice. (Adapted from Tewes et al., "Functional MRI for characterization of renal perfusion impairment and edema formation due to acute kidney injury in different mouse strains" PloS One)

inflammation response. The persisting T_1 increase in severe AKI may at least partly be explained by development of fibrosis due to inadequate renal tissue regeneration and incomplete tubular repair. In a follow-up study, changes in T_1 (and arterial spin labeling perfusion parameters) after AKI was assessed in two mouse strains (C57BL/6 and 129/Sv) to investigate potential effects of different genetic backgrounds on the experimental study [5]. Overall, similar trends of increased T_1 were found in both animal models, except for a significantly higher T_1 increase in the cortex and outer stripe of the outer medulla (OSOM) of the 129/Sv vs. C57BL/6 mice at day 1 after moderate AKI and higher relative T_1 values in the cortex and lower relative T_1 values in the inner stripe of the outer medulla (ISOM) at day 7 after severe AKI in 129/Sv mice (Fig. 4) The same research team also assessed multiparametric MRI parameters, including T_1, in mouse models of allogenic and isogenic renal

transplantation [2]. Acute allograft rejection was observed in allogenic kidney transplants. T_1 was significantly elevated in allogenic vs. isogenic allografts. Histopathological evaluation showed signification strong correlations of T_1 with presence of macrophages, T-cells and fibrosis (correlation coefficient r range 0.78–0.91, $P < 0.01$). These studies show that kidney T_1 is sensitive to several pathophysiological processes, including inflammation and fibrosis, which may occur simultaneously in events of kidney injury and rejection.

The findings of the group of Hueper et al. have also been observed by other research groups in independent studies. Jiang et al. employed longitudinal multiparametric MRI, including T_1 for evaluation of folic acid-induced AKI in mice [4]. The experiments were performed at a 16.4 T dedicated animal MR system (Bruker). T_1 was found to increase in both the renal cortex and medulla, most prominently at 2 weeks after treatment, while T_1 tended to regress at 4 weeks after treatment. Histopathological evaluation showed increased fluid content and association of tubular dilation at 2 weeks after treatment, explaining the T_1 elevation.

While dedicated preclinical MRI systems are highly suitable for high-resolution imaging of kidneys in small animals, clinical systems could also be used for preclinical renal T_1 studies. Ko et al. performed a longitudinal multiparametric MRI study after severe bilateral ischemic-reperfusion AKI in rat kidneys on a clinical 3 T MR scanner [28]. T_1 values were elevated in both the cortex and medulla after AKI, similar as reported in previous studies. No significant correlations of T_1 with histopathological evaluation of different markers including macrophages and collagen deposition were observed, possibly owing to complex pathological changes after AKI and multiple factors attributing to the T_1 changes. Hu et al. found significant positive correlations of T_1 with histological expression of Masson's trichrome (collagen) and alpha-smooth muscle actin in a multiparametric MRI study in a rat model of unilateral ureteral obstruction performed on a clinical 3 T MRI system [29]. Friedli et al. also found significant correlations of T_1 with histopathological inflammation and fibrosis in a rat model of unilateral ureteral obstruction. The latter study was performed on a 3 T MR system [20].

Gao et al. have reported feasibility of MR fingerprinting for imaging of healthy mouse kidneys on a preclinical 7 T MR system, showing inherent resistance of the MR fingerprinting technique to respiratory motion artifacts [30].

T_1 may also be used as baseline measurement for DCE-MRI acquisitions. More information on the use of T_1 for quantitative DCE-MRI measurements can be found in the chapters by Pedersen M et al. "Dynamic Contrast Enhancement (DCE) MRI–Derived Renal Perfusion and Filtration: Basic Concepts"; by Irrera P et al. "Dynamic Contrast Enhanced (DCE) MRI-Derived Renal

Perfusion and Filtration: Experimental Protocol"; and by Zöllner FG et al. "Analysis Protocol for Dynamic Contrast Enhanced (DCE) MRI of Renal Perfusion and Filtration," which cover the basic concept, experimental protocols, and analysis techniques of DCE-MRI, respectively.

In summary, several studies have demonstrated suitability of T_1 for assessment of renal pathology in preclinical models. These promising results warrant further investigation of this MRI relaxation technique both in the preclinical and clinical settings.

Acknowledgement

The experiments shown in Fig. 3 were performed on a platform member of France Life Imaging network (grant ANR-11-INBS-0006).

This chapter is based upon work from COST Action PARENCHIMA, supported by European Cooperation in Science and Technology (COST). COST (www.cost.eu) is a funding agency for research and innovation networks. COST Actions help connect research initiatives across Europe and enable scientists to enrich their ideas by sharing them with their peers. This boosts their research, career, and innovation.

PARENCHIMA (renalmri.org) is a community-driven Action in the COST program of the European Union, which unites more than 200 experts in renal MRI from 30 countries with the aim to improve the reproducibility and standardization of renal MRI biomarkers.

References

1. Selby NM, Blankestijn PJ, Boor P, Combe C, Eckardt KU, Eikefjord E, Garcia-Fernandez N, Golay X, Gordon I, Grenier N, Hockings PD, Jensen JD, Joles JA, Kalra PA, Kramer BK, Mark PB, Mendichovszky IA, Nikolic O, Odudu A, Ong ACM, Ortiz A, Pruijm M, Remuzzi G, Rorvik J, de Seigneux S, Simms RJ, Slatinska J, Summers P, Taal MW, Thoeny HC, Vallee JP, Wolf M, Caroli A, Sourbron S (2018) Magnetic resonance imaging biomarkers for chronic kidney disease: a position paper from the European Cooperation in Science and Technology action PARENCHIMA. Nephrol Dial Transplant 33(suppl_2):ii4–ii14. https://doi.org/10.1093/ndt/gfy152
2. Hueper K, Hensen B, Gutberlet M, Chen R, Hartung D, Barrmeyer A, Meier M, Li W, Jang MS, Mengel M, Wacker F, Rong S, Gueler F (2016) Kidney transplantation: multiparametric functional magnetic resonance imaging for assessment of renal allograft pathophysiology in mice. Investig Radiol 51(1):58–65. https://doi.org/10.1097/RLI.0000000000000205
3. Hueper K, Peperhove M, Rong S, Gerstenberg J, Mengel M, Meier M, Gutberlet M, Tewes S, Barrmeyer A, Chen R, Haller H, Wacker F, Hartung D, Gueler F (2014) T1-mapping for assessment of ischemia-induced acute kidney injury and prediction of chronic kidney disease in mice. Eur Radiol 24(9):2252–2260. https://doi.org/10.1007/s00330-014-3250-6
4. Jiang K, Ponzo TA, Tang H, Mishra PK, Macura SI, Lerman LO (2018) Multiparametric MRI detects longitudinal evolution of folic acid-induced nephropathy in mice. Am J Physiol Renal Physiol 315(5):F1252–F1260. https://doi.org/10.1152/ajprenal.00128.2018

5. Tewes S, Gueler F, Chen R, Gutberlet M, Jang MS, Meier M, Mengel M, Hartung D, Wacker F, Rong S, Hueper K (2017) Functional MRI for characterization of renal perfusion impairment and edema formation due to acute kidney injury in different mouse strains. PLoS One 12(3):e0173248. https://doi.org/10.1371/journal.pone.0173248
6. Maril N, Margalit R, Rosen S, Heyman SN, Degani H (2006) Detection of evolving acute tubular necrosis with renal 23Na MRI: studies in rats. Kidney Int 69(4):765–768. https://doi.org/10.1038/sj.ki.5000152
7. Haacke EM, Brown RW, Thompson MR, Venkatesan R (1999) Magnetic resonance imaging: physical principles and sequence design. Wiley, New York
8. Nishimura DG (1996) Principles of magnetic resonance imaging. Stanford University, Stanford, CA
9. Brown RW, Cheng Y-CN, Haacke EM, Thompson MR, Venkatesan R (2014) Magnetic resonance imaging: physical principles and sequence design, 2nd edn. Wiley-Blackwell, New York, NY
10. Berger S, Braun S (2004) 200 and more NMR experiments: a practical course, 1st edn. Wiley-VCH
11. Kierulf-Lassen C, Nielsen PM, Qi H, Damgaard M, Laustsen C, Pedersen M, Krag S, Birn H, Norregaard R, Jespersen B (2017) Unilateral nephrectomy diminishes ischemic acute kidney injury through enhanced perfusion and reduced pro-inflammatory and pro-fibrotic responses. PLoS One 12(12):e0190009. https://doi.org/10.1371/journal.pone.0190009
12. Little RA, Jamin Y, Boult JKR, Naish JH, Watson Y, Cheung S, Holliday KF, Lu H, McHugh DJ, Irlam J, West CML, Betts GN, Ashton G, Reynolds AR, Maddineni S, Clarke NW, Parker GJM, Waterton JC, Robinson SP, O'Connor JPB (2018) Mapping hypoxia in renal carcinoma with oxygen-enhanced MRI: comparison with intrinsic susceptibility MRI and pathology. Radiology 288(3):739–747. https://doi.org/10.1148/radiol.2018171531
13. Kingsley P (1999) Methods of measuring spin-lattice (t1) relaxation times: an annotated bibliography. Concepts Magn Reson 11:243–276. https://doi.org/10.1002/(SICI)1099-0534
14. Stikov N, Boudreau M, Levesque IR, Tardif CL, Barral JK, Pike GB (2015) On the accuracy of T1 mapping: searching for common ground. Magn Reson Med 73(2):514–522. https://doi.org/10.1002/mrm.25135
15. Fennessy FM, Fedorov A, Gupta SN, Schmidt EJ, Tempany CM, Mulkern RV (2012) Practical considerations in T1 mapping of prostate for dynamic contrast enhancement pharmacokinetic analyses. Magn Reson Imaging 30(9):1224–1233. https://doi.org/10.1016/j.mri.2012.06.011
16. Aryal MP, Chenevert TL, Cao Y (2016) Impact of uncertainty in longitudinal T1 measurements on quantification of dynamic contrast-enhanced MRI. NMR Biomed 29(4):411–419
17. Schabel MC, Parker DL (2008) Uncertainty and bias in contrast concentration measurements using spoiled gradient echo pulse sequences. Phys Med Biol 53(9):2345–2373. https://doi.org/10.1088/0031-9155/53/9/010
18. Raman FS, Kawel-Boehm N, Gai N, Freed M, Han J, Liu CY, Lima JA, Bluemke DA, Liu S (2013) Modified Look-Locker inversion recovery T1 mapping indices: assessment of accuracy and reproducibility between magnetic resonance scanners. J Cardiovasc Magn Reson 15:64. https://doi.org/10.1186/1532-429x-15-64
19. Roujol S, Weingartner S, Foppa M, Chow K, Kawaji K, Ngo LH, Kellman P, Manning WJ, Thompson RB, Nezafat R (2014) Accuracy, precision, and reproducibility of four T1 mapping sequences: a head-to-head comparison of MOLLI, ShMOLLI, SASHA, and SAPPHIRE. Radiology 272(3):683–689. https://doi.org/10.1148/radiol.14140296
20. Friedli I, Crowe LA, Berchtold L, Moll S, Hadaya K, de Perrot T, Vesin C, Martin PY, de Seigneux S, Vallee JP (2016) New magnetic resonance imaging index for renal fibrosis assessment: a comparison between diffusion-weighted imaging and T1 mapping with histological validation. Sci Rep 6:30088. https://doi.org/10.1038/srep30088
21. Look DC, Locker D (1970) Time saving in measurement of NMR and EPR relaxation times. Rev Sci Instrum 41:250–251
22. Huang W, Wang Y, Panicek DM, Schwartz LH, Koutcher JA (2009) Feasibility of using limited-population-based average R10 for pharmacokinetic modeling of osteosarcoma dynamic contrast-enhanced magnetic resonance imaging data. Magn Reson Imaging 27(6):852–858. https://doi.org/10.1016/j.mri.2009.01.020
23. Ma D, Gulani V, Seiberlich N, Liu K, Sunshine JL, Duerk JL, Griswold MA (2013) Magnetic resonance fingerprinting. Nature 495(7440):187–192. https://doi.org/10.1038/nature11971

24. Wolf M, de Boer A, Sharma K, Boor P, Leiner T, Sunder-Plassmann G, Moser E, Caroli A, Jerome NP (2018) Magnetic resonance imaging T1- and T2-mapping to assess renal structure and function: a systematic review and statement paper. Nephrol Dial Transplant 33(suppl_2):ii41–ii50. https://doi.org/10.1093/ndt/gfy198
25. Abrashkin S, Weininger J, Griffel L, Schneider R, Iaina A (1987) Proton magnetic resonance in experimental acute and chronic renal failure in rats. Ren Fail 10(1):21–27
26. Iaina A, Abrashkin S, Weininger J (1986) Proton MR study of different types of experimental acute renal failure in rats. Magn Reson Imaging 4(3):241–244
27. Loupy A, Haas M, Solez K, Racusen L, Glotz D, Seron D, Nankivell BJ, Colvin RB, Afrouzian M, Akalin E, Alachkar N, Bagnasco S, Becker JU, Cornell L, Drachenberg C, Dragun D, de Kort H, Gibson IW, Kraus ES, Lefaucheur C, Legendre C, Liapis H, Muthukumar T, Nickeleit V, Orandi B, Park W, Rabant M, Randhawa P, Reed EF, Roufosse C, Seshan SV, Sis B, Singh HK, Schinstock C, Tambur A, Zeevi A, Mengel M (2017) The Banff 2015 kidney meeting report: current challenges in rejection classification and prospects for adopting molecular pathology. Am J Transplant 17(1):28–41. https://doi.org/10.1111/ajt.14107
28. Ko SF, Yip HK, Zhen YY, Lee CC, Lee CC, Huang SJ, Huang CC, Ng SH, Lin JW (2017) Severe bilateral ischemic-reperfusion renal injury: hyperacute and acute changes in apparent diffusion coefficient, T1, and T2 mapping with immunohistochemical correlations. Sci Rep 7(1):1725. https://doi.org/10.1038/s41598-017-01895-x
29. Hu G, Liang W, Wu M, Lai C, Mei Y, Li Y, Xu J, Luo L, Quan X (2018) Comparison of T1 mapping and T1rho values with conventional diffusion-weighted imaging to assess fibrosis in a rat model of unilateral ureteral obstruction. Acad Radiol 26(1):22–29. https://doi.org/10.1016/j.acra.2018.03.023
30. Gao Y, Chen Y, Ma D, Jiang Y, Herrmann KA, Vincent JA, Dell KM, Drumm ML, Brady-Kalnay SM, Griswold MA, Flask CA, Lu L (2015) Preclinical MR fingerprinting (MRF) at 7 T: effective quantitative imaging for rodent disease models. NMR Biomed 28(3):384–394. https://doi.org/10.1002/nbm.3262